Abstract We describe an asymptotic model for the behavior of PET-like heat-shrinkable thin films that includes both membrane and bending energies when the thickness of the film is positive. We compare the model to Koiter's shell model and to models in which a membrane energy or a bending energy are obtained by Γ-convergence techniques. We also provide computational results for various temperature distributions applied to the films.

Keywords Thin film · Heat shrinking · Membrane energy · Bending energy · Melinex® · Compatibility conditions

Mathematics Subject Classification (2000) 74B15 · 74B20 · 74F05 · 74G65 · 74K35 · 74S05 · 93B40

Noname manuscript No.
(will be inserted by the editor)

Modeling the behavior of heat-shrinkable thin films

Pavel Bělík · Bob Jennings · Mikhail M. Shvartsman · Cristina U. Thomas

January 28, 2009

1 Introduction

In this paper we attempt to analyze the behavior of heat-shrinkable thin films. The material of the film could be of general nature; however, the industrial motivation for this work comes from heat-shrinking polymeric thin films onto car windshields. These films are well represented by materials such as PET. Constitutive description of polymers invokes numerous mathematical and modeling challenges due to the complicated configuration of polymer molecules. The main feature we are interested in here is the ability of polymers to shrink at high temperatures. A rough explanation for this effect is that heating increases the ability of molecules to rearrange atoms comprising the molecules in such a way that the total internal energy is minimized. Our goal is to define a simple, yet descriptive enough energy to be minimized to capture the resulting deformation of the film. One might hope that a modeling approach based on minimization of energy allows one not only to find a state with (locally) minimal energy, but also (assuming the molecule rearrangement happens on a much shorter time scale than other effects of interest in this paper) possibly trace the dynamics of evolution through the energy-minimizing sequences of configurations of the thin film.

Pavel Bělík
Mathematics Department, Campus Box 93, Augsburg College, 2211 Riverside Ave, Minneapolis, MN 55454, U.S.A.
E-mail: belik@augsburg.edu

Bob Jennings
Structural Adhesives BTO, 3M Center Bldg 230-1G-06, Maplewood, MN 55144, U.S.A.
E-mail: bjennings1@mmm.com

Mikhail M. Shvartsman
Department of Mathematics, University of St. Thomas, 2115 Summit Avenue, St. Paul, MN 55105, U.S.A.
E-mail: mmshvartsman@stthomas.edu

Cristina U. Thomas
Safety, Security and Protection Services Business Laboratory, 3M Center Bldg 201-2S-05, Maplewood, MN 55144, U.S.A.
E-mail: cuthomas@mmm.com

For materials with memory, the general constitutive equation for stress at time t should respect the history of the strain evolution and the temperature evolution up to time t and hence one might write (see,e.g., [2, 27])

$$\sigma(x,t) = \hat{\sigma}\left(E(x,\cdot), \theta(x,\cdot)\right),$$

where $\sigma(x,t)$ is the stress at time t at the point x in the reference configuration, $E(x,\cdot)$ denotes the strain at the point x with its history up to time t, and $\theta(x,\cdot)$ denotes the temperature at the point x with its history up to time t. An example of such a relationship without the dependence on temperature history is given by a single integral of the form

$$\sigma(x,t) = \int_0^t m(x,t-\tau)\frac{\partial E}{\partial \tau}(x,\tau)\, d\tau,$$

where $m(x,t-\tau)$ represents a relaxation modulus. Relationships like the one above have been used in literature (see, e.g., [18, 26, 28, 37, 38, 40, 45]), but they are in general quite complicated and are often replaced by viscoelastic and/or thermo-viscoelastic approximations that depend on the values of the strain and the temperature as well as their time derivatives at time t (see, e.g., [2, 27])

$$\sigma(x,t) = \hat{\sigma}\left(E(x,t), \frac{\partial E}{\partial t}(x,t), \theta(x,t), \frac{\partial \theta}{\partial t}(x,t)\right)$$

that allow one to avoid complicated integro–differential equations in the formulation of a boundary-value problem or a corresponding minimization problem.

The materials modeled in our paper are represented by a DuPont's Melinex® polyester film. Polyester is an example of a material, for which it is reasonable to (locally) decouple time and strain [39] due to the special dynamics of hysteresis in the evolution of strain. The experiments presented in Section 2 demonstrate that the reversible part of strain can be separated from the plasticity effects for the particular temperature distribution across the film that leads to the behavior shown in Figures 1 and 2. That is, one can assume that the relaxation effects are taking place only at high temperatures, and so all the relaxation and hysteretic effects are avoided at low temperatures.

Based on the results of the experiments described in Section 2, the class of materials represented by Melinex® exhibit an isotropic strain–temperature relationship when the material is *uniformly* heated above a certain critical temperature and then cooled down to the room temperature. The film's response seems affected only by the highest temperature the film has experienced. This leads us to introduce in Section 3 in equation (1) the concept of a locally "preferred" Cauchy–Green strain for a given attained maximum temperature, and in (3) an energy density as a function of the difference between the actual Cauchy–Green strain and the "preferred" Cauchy–Green strain denoted by $2E$, i.e., E represents one-half of the deviation of the actual Cauchy–Green strain from the preferred strain. This conveniently bypasses having to deal directly with stress, yet the stress can still be computed, if needed, from the energy density.

Our goal is to study the behavior of thin films of these materials. There is a vast amount of literature on the subject of thin films, and one of the recent popular techniques of 3D to 2D reduction is that of Γ-convergence, whereby a limit of a general three-dimensional energy functional and its minimizers are studied as the thickness of the film tends to zero (see, e.g., [1, 3–5, 14, 19, 22, 23, 31, 34, 36, 44]). Since the Γ-limit

of the energy of an asymptotically thin film is a two-dimensional energy, it can provide a more tractable and efficiently computed model. However, the films of interest in the industry have finite, nonnegligible thickness on the order of 10 μm–500 μm, and therefore a competition between a membrane energy and a bending energy will take place. Since these two energies are of different orders of magnitude in the thickness of the film, Γ-convergence techniques cannot recover both of them simultaneously.

Other models, mostly based on asymptotic expansions, have been proposed and studied in the literature (see, e.g., [29,30,33,46,47]) that combine both the membrane and bending energies. Our approach in Section 3 is based on the asymptotic expansion of the deformation of the film with as few assumptions as possible. We introduce an energy model (see (12) and (13)) that has as its first two lowest-order terms a "membrane" energy of order h (where h is the thickness of the film) and a "bending" energy of order h^3. In Sections 4 and 5 we compare the membrane and bending energies from our model to those obtained by Γ-convergence techniques and those in the popular Koiter's shell model, respectively. In order to make these comparisons, we assume that no temperature-induced shrinkage takes place, and show that in both cases the bending energies agree, while there is are slight disagreements in the membrane energy expressions. Finally, in Section 6, we use a simplified version of our model and present some results of computer simulations for free-standing films subjected to various temperature distributions.

Our approach in this paper is similar in effect to that in [46] and [47]. We start assuming that the deformation of the film can be asymptotically expanded in the out-of-plane variable and arrive at an expansion of the relevant energy in the thickness of the film. In [46], the starting point is an asymptotic expansion of the deformation in the thickness of the film, and the outcome is an expansion of energy. In [47], the starting point is an asymptotic expansion of the energy in the thickness of the film and the results can be interpreted in terms of the expansion of the deformation. We also note that unlike in [29,30], our model depends only on the strain associated with the deformation, not the gradient of the strain.

2 Description of experimental data

Experiments have been performed in 3M laboratories to measure the non-reversible shrinkage behavior of DuPont's Melinex® polyester films. As most films of this type, they exhibit a reversible thermal expansion behavior with a non-reversible dimensional instability superimposed as a result condition in the film processing. For many films, such as these, the dimensional instability is often intentionally tuned into the film to enhance its performance in the particular application it is intended for. The sources of the shrinkage are often viscoelastic in nature and in the case of semi-crystalline polymers are often tied to the melting of crystalline physical crosslinks as well. Overall the behavior is tied to a combination of the material properties and particular stress history of the film.

Whichever the case, the shrinkage behavior can be observed and measured by heating strips of the film through various heating cycles while measuring the film length. Generally, on the first heat the film displays shrinkage behavior superimposed on the thermal expansion behavior. During cooldown the film usually displays only reversible thermal expansion. On subsequent heats, the film displays only the reversible thermal expansion behavior up until the highest temperature of the previous heating cycle, then

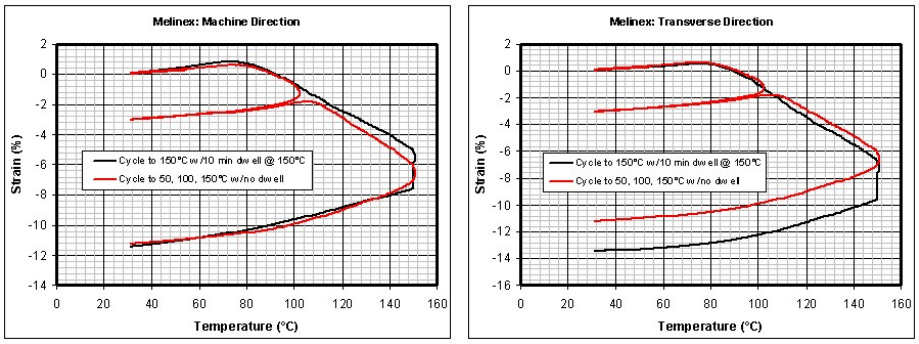

Fig. 1 Results of the heating and cooling of the Melinex® film. The plots show strain (relative elongation) in the particular direction as a function of temperature. The black curves correspond to heating the film up to 150°C and cooling it down to 30°C with a 10-minute dwell at 150°C. The red curves correspond to heating/cooling cycles from 30°C to 50°C to 30°C, from 30°C to 100°C to 30°C, and from 30°C to 150°C to 30°C with no dwell at the highest temperatures. Note the purely elastic response in the 30–50–30 cycle.

it goes on to display a combination of thermal expansion and non-reversible shrinkage at higher temperatures as chain movements associated with longer relaxation times kick in.

For this particular study, strips of Melinex® polyester film of thickness 50.8 μm (2 mil) of approximate sizes 2.5 cm by 0.3 cm were cut from a master roll in both the machine and transverse directions of the film. Each strip was placed in a TA Instruments 2940 Thermal Mechanical Analyzer (TMA) fitted with a Film and Fiber Probe. A small load of approximately 0.005 kg was imposed on the strip to keep it straight and the specimen was also subjected to a heating regimen consisting of (1) heating at a rate of 5°C/min to 150°C, (2) holding at 150°C for 10 minutes, and (3) cooling back to 30°C at a nominal rate of −5°C/min. The 5°C/min cooling rate could be maintained for temperatures above 100°C, but it generally slowed down at the lower temperatures due to the room-temperature air used to cool the chamber. Although techniques exist to speed up the process on this machine using liquid nitrogen, we have generally found that the mechanical noise and vibrations often create excessive noise in the shrinkage data, while the slower cooling rates at the lower temperatures generally do not affect the measurement results. Plots of percent strain (referenced to the initial sample length at 30°C) versus temperature for specimens cut in the machine and transverse directions are shown as black curves in Fig. 1. Both plots show a gradual length increase of the specimens with temperature up to about 80°C followed by a gradual shrinkage from 80°C to 150°C. The specimens continue to shrink slightly during the isotherm at 150°C, then shrink again as they are cooled back to 30°C.

To demonstrate the behavior of the non-reversible shrinkage discussed above, a second set of specimens were placed in the TMA and subjected to a slightly different heating regime consisting of three heating cycles running to progressively higher temperatures of 50°C, 100°C, and 150°C at 5°C/min but with no isothermal stages. During the first cycle to 50°C, the heating and cooling curves superimposed on one another indicated only reversible thermal expansion behavior exhibited by the material up to that temperature. In the next cycle to 100°C, the specimens showed nearly identical behavior to the original cycle to 150°C and showed the reversible thermal

contraction upon cooling from 100°C. During the last cycle to 150°C, the length of the specimen tracked exactly with the cooling curve from the previous cycle, then displayed non-reversible shrinkage again at temperatures above 100°C, the highest temperature of the previous cycle. For the remainder of the final cycle the strain-versus-temperature behavior tracked with that displayed by specimens in the single cycle heat to 150°C. These results are displayed as red curves in Fig. 1.

A notable exception to the tracking behavior between the single- and multiple-cycle routines is seen in the specimens cut in the transverse direction. There we can see the impact of the 10-minute dwell at 150°C on the total shrinkage. Ironically, it is this sample that is displaying the expected behavior, while the specimens cut in the machine direction more closely tracking at the higher temperatures and final cooldown are displaying the slightly anomalous behavior. We have no explanation of this other than probable differences in specimen handling or loading in the TMA. Since we are largely concerned with specimen behavior up to about 100°C and not higher, we were not too concerned about the differences displayed under the more unstable conditions at the higher temperatures.

For this study we are primarily interested in quantifying the non-reversible shrinkage behavior of the film for use in the shaping model. In other words, we want to know how much the film will shrink in a given direction after being exposed to some elevated temperature and then cooled down to the room temperature. To isolate this behavior, we simply identify the cooling behavior during the final cooldown of our specimens from 150°C as reversible thermal expansion. We then subtract this curve (offset to zero at 30°C) from the previous heating curves to produce the plots shown in Fig. 2. In this treatment we essentially ignore all time-dependent effects. This treatment is reasonably valid as long as we qualify all predictions as occurring on a similar time scale as our measurements, and as long as we do not go to too high temperatures (say above 100°C or so in this case.) The plots in Fig. 2 show the expected non-reversible shrinkage of the film as a function of temperature. That is, specimens heated up to about 70°C (and not held at that temperature for an excessive period of time) are not expected to display any shrinkage after cooling. However, specimens heated to about 100°C are expected to shrink approximately 2% in the machine direction and approximately 3% in the transverse direction. The multiple-cycle plot reveals the error in the machine direction data. In that case, the single-cycle curve appears to predict slightly less shrinkage than measured by the multiple-cycle plot. Judging from comparisons of the multiple-cycle plots in both the machine and transverse directions, it appears that the shrinkage behavior in the film is roughly the same in both directions and predicted more precisely by the curve produced in the transverse direction.

3 Description of the model

We shall assume that the reference configuration of the undistorted film with thickness $h > 0$ is $\Omega_h = \Omega \times \left(-\frac{h}{2}, \frac{h}{2}\right)$, where $\Omega \subset \mathbb{R}^2$ is a domain with a Lipschitz continuous boundary, $\partial\Omega$. The film will be assumed to undergo a (non-self-intersecting) deformation $u : \Omega_h \to \mathbb{R}^3$ with the deformation gradient $F = \nabla u : \Omega_h \to \mathbb{R}^{3\times 3}$ (such that $\det F > 0$) and the right Cauchy–Green strain $C = F^T F = (\nabla u)^T \nabla u : \Omega_h \to \mathbb{R}^{3\times 3}$.

Based on the experimental results in the previous section, we shall make the assumption that the local response of the film is a function of the highest temperature the material point in question has experienced so far. One of our working assumptions

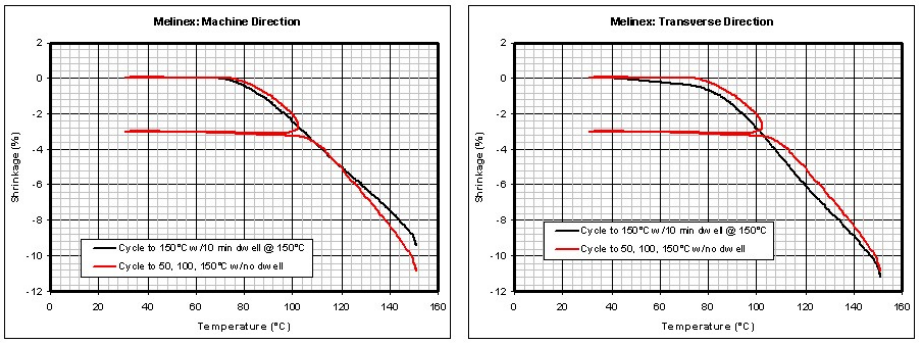

Fig. 2 Results of the heating and cooling of the Melinex® film. The plots show the actual percentual shrinkage of the film at the end of the heating/cooling cycle as a function of the highest temperature the film is exposed to. The black curves correspond to heating the film up to 150°C and cooling it down to 30°C with a 10-minute dwell at 150°C. The red curves correspond to heating/cooling cycles from 30°C to 50°C to 30°C, from 30°C to 100°C to 30°C, and from 30°C to 150°C to 30°C with no dwell at the highest temperatures. Note the purely elastic response in the 30–50–30 cycle.

will be that the film is thin enough so that heat diffusion within the film does not play a significant role in heat transfer, and therefore, after heating (using, for example, a heat gun as in the experiments described in Section 2), most of the heat escapes quickly into the surrounding cooler air. Under this assumption, the only role of the heat treatment is to "prescribe" or "imprint" a certain non-uniformity into the material in order to control its shrinkage. In addition, we remark that the experimentally observed and visually significant deformation that took place after the film was heated up was almost instantaneous, indicating that the time scale for the deformation would be much shorter than a relevant time scale for heat diffusion.

With this understanding, we shall now assume that the material can be modeled by a stored energy functional. To construct an energy model that accommodates large rotations, we shall utilize the geometrically nonlinear continuum theory. Thus, the stored energy density per unit volume will be a frame-indifferent function of the deformation gradient, F; using the polar decomposition theorem [2], frame indifference implies that the energy density is a function of the Cauchy–Green strain, C. Based on the discussion in the previous section, we shall assume that a uniformly heated (and then cooled down to room temperature) material would undergo a uniform deformation with the right Cauchy–Green strain $I(\theta) \in \mathbb{R}^{3\times 3}$, where $\theta \in \mathbb{R}$ denotes the maximum applied temperature. For low maximum temperatures, we have $I(\theta) = I$ (the 3×3 identity matrix) as there is no shrinkage. For high temperatures and isotropic materials,

$$I(\theta) = (1 - f(\theta))I \tag{1}$$

for a suitable function $0 \leq f(\theta) < 1$. We shall therefore assume that $I(\theta)$ represents a zero-energy state, an energetically "preferred" Cauchy–Green strain. To capture the dependence of the energy on the strain and the temperature, we shall assume that the energy density is an integrable function $W : \mathbb{R}^{3\times 3} \times \mathbb{R} \to \mathbb{R}_+$, i.e., it is a nonnegative function of two arguments, the right Cauchy–Green strain, C, and the temperature, θ. Motivated by the definition of the Green–St. Venant strain (given by $\frac{1}{2}(C - I)$), we define a corresponding quantity as one-half of the difference between the Cauchy–Green

strain and the "preferred" Cauchy–Green strain,

$$E(\theta) = \frac{1}{2}(C - I(\theta)), \tag{2}$$

and define the energy density to be a function of the form

$$W(C, \theta) = \tilde{W}(E)\big|_{E=\frac{1}{2}(C-I(\theta))} \tag{3}$$

with $\tilde{W}$ being a nonnegative function defined on symmetric 3×3 matrices, and $\tilde{W}(E) = 0$ if and only if $E = 0$.

To demonstrate simple concepts below and for computational purposes in Section 6, we shall use a quadratic energy density of the form

$$\tilde{W}(E) = \frac{1}{2}E \cdot \mathbb{C}E, \tag{4}$$

where $\mathbb{C}$ is the symmetric, positive definite elasticity tensor. The matrix dot product is defined in the usual way

$$A \cdot B = \operatorname{tr}(A^T B) \qquad \text{for } A, B \in \mathbb{R}^{3\times3}.$$

The total stored energy, $\mathcal{E}_h$, of the film of thickness h, as a function of the deformation u and the temperature θ, is now given by[1]

$$\mathcal{E}_h(u, \theta) = \int_{\Omega_h} W(\nabla u(x)^T \nabla u(x), \theta(x))\, dx.$$

Using the expressions (2)–(4), the energy of the film becomes

$$\begin{aligned} \mathcal{E}_h(u, \theta) &= \int_{\Omega_h} \tilde{W}\left(\tfrac{1}{2}(C(x) - I(\theta(x))\right) dx \\ &= \int_{\Omega_h} \frac{1}{8}\left[C(x) - I(\theta(x))\right] \cdot \mathbb{C}\left[C(x) - I(\theta(x))\right]\, dx, \end{aligned} \tag{5}$$

where $C(x) = \nabla u(x)^T \nabla u(x)$. Since the elasticity tensor, $\mathbb{C}$, is symmetric, positive definite, it follows that the total stored energy is zero if and only if the deformation is such that the material at *almost every* material point experiences the shrinkage it would if the film was *globally* heated to the same temperature as the point experiences, i.e., if $C(x) = I(\theta(x)) = (1 - f(\theta(x)))\, I$. The question then arises whether there exists a deformation that associates with such a Cauchy–Green strain field. The compatibility conditions which allow this possibility put a severe restriction on the tensor $I(\theta(x))$, and hence on the temperature distribution, $\theta(x)$ [16]. Due to a famous theorem of Liouville concerning conformal maps in $\mathbb{R}^n$ (restricted to $n = 3$), the assumption $C(x) = I(\theta(x))$ implies that either $I(\theta(x))$ is constant throughout the film's reference configuration, or $I(\theta(x)) = \alpha^2|x - \tilde{x}|^{-4} I$ for a nonzero constant α and a point $\tilde{x} \in \mathbb{R}^3$. The first case, $I(\theta(x))$ being constant, implies that either the temperature is constant throughout the body, or it varies arbitrarily in the interval corresponding to no shrinkage. Neither

[1] For simplicity of the treatment, we assume that the temperature field can be prescribed in the reference configuration. When the resulting deformations are small, this approach should introduce only small errors. Alternatively, one can think of a human operator following the material point as the film deforms. This is a current practice in 3M when applying the films onto car windshields.

scenario is very interesting in applications as they represent uniform shrinkage, and no shrinkage, respectively. It can be shown that in the second case a Cauchy–Green strain of the form $I(\theta(x)) = \alpha^2|x-\tilde{x}|^{-4}I$ corresponds to a deformation of the form

$$u(x) = \alpha\, A\, \frac{x-\tilde{x}}{|x-\tilde{x}|^2} + \hat{x},$$

where $\hat{x} \in \mathbb{R}^3$ and $A \in \mathrm{O}(3)$ is such that $\det(\alpha A) < 0$; that is, this deformation is an inversion combined with rotation, uniform stretching or shrinking, and translation. Outside of these very special cases, the compatibility condition $C(x) = I(\theta(x))$ cannot be satisfied and one cannot expect to find zero-energy deformations. In those cases, residual stresses will be present in energy-minimizing deformations.

In what follows, we shall try to address the issue of this restrictive compatibility condition by focusing on the thinness of the film and approximating the full 3D model by a 2D model. To start with, we make some simplifying assumptions about the deformation that the film can undergo. Motivated by the outcomes of various thin film results (e.g., [1, 3–5, 14, 19, 22, 23, 29–31, 34, 36, 44, 46, 47]), we shall assume that the deformation $u : \Omega_h \to \mathbb{R}^3$ can be expanded around the middle surface[2] $\Omega \times \{0\}$

$$\begin{aligned} u(x_1,x_2,x_3) = u(x_1,x_2,0) + x_3\frac{\partial u}{\partial x_3}(x_1,x_2,0) + \frac{x_3^2}{2}\frac{\partial^2 u}{\partial x_3^2}(x_1,x_2,0) \\ + \frac{x_3^3}{6}\frac{\partial^3 u}{\partial x_3^3}(x_1,x_2,0) + o(x_3^3) \qquad \text{as } x_3 \to 0. \end{aligned} \tag{6}$$

If we make the identification

$$\begin{aligned} y(x_1,x_2) &= u(x_1,x_2,0), \\ b(x_1,x_2) &= \frac{\partial u}{\partial x_3}(x_1,x_2,0), \\ c(x_1,x_2) &= \frac{\partial^2 u}{\partial x_3^2}(x_1,x_2,0), \\ d(x_1,x_2) &= \frac{\partial^3 u}{\partial x_3^3}(x_1,x_2,0), \end{aligned} \tag{7}$$

so that we can write

$$u(x_1,x_2,x_3) = y(x_1,x_2) + x_3 b(x_1,x_2) + \frac{x_3^2}{2}\,c(x_1,x_2) + \frac{x_3^3}{6}\,d(x_1,x_2) + o(x_3^3)$$

as $x_3 \to 0$, and if we neglect the highest-order term, we have that as $x_3 \to 0$

$$F = \nabla u(x_1,x_2,x_3) = \big(y_{,1}|y_{,2}|b\big) + x_3\,\big(b_{,1}|b_{,2}|c\big) + \frac{x_3^2}{2}\,\big(c_{,1}|c_{,2}|d\big)\,. \tag{8}$$

In the above, we have used the notation $f_{,i} = \frac{\partial f}{\partial x_i} = (\frac{\partial f_1}{\partial x_i}, \frac{\partial f_2}{\partial x_i}, \frac{\partial f_3}{\partial x_i})^T$ for a function $f : \mathbb{R}^3 \to \mathbb{R}^3$, and $A = (A_1|A_2|A_3)$ for $A \in \mathbb{R}^{3\times 3}$, where the A_i denote the columns of A. If we now denote the matrix terms in (8) by F_0, F_1, and F_2, respectively, i.e.,

$$\begin{aligned} F_0 &= \big(y_{,1}|y_{,2}|b\big)\,, \\ F_1 &= \big(b_{,1}|b_{,2}|c\big)\,, \\ F_2 &= \big(c_{,1}|c_{,2}|d\big)\,, \end{aligned} \tag{9}$$

[2] As in [25], one might start with the expansion in x_3 and h simultaneously and find the energy-minimizing coefficients. Due to the simple geometry considered in this case, with the middle surface corresponding to $x_3 = 0$, this expansion would reduce to the one given in (6).

and if in addition we define

$$\begin{aligned} C_0 &= F_0^T F_0, \\ C_1 &= F_0^T F_1 + F_1^T F_0, \\ C_2 &= F_0^T F_2 + F_2^T F_0 + 2\, F_1^T F_1, \end{aligned} \tag{10}$$

we get that as $x_3 \to 0$ the Cauchy–Green strain satisfies

$$\begin{aligned} C = F^T F &= \left(F_0 + x_3 F_1 + \frac{x_3^2}{2} F_2\right)^T \left(F_0 + x_3 F_1 + \frac{x_3^2}{2} F_2\right) + o(x_3^2) \\ &= F_0^T F_0 + x_3 (F_0^T F_1 + F_1^T F_0) + \frac{x_3^2}{2} \left(F_0^T F_2 + F_2^T F_0 + 2\, F_1^T F_1\right) + o(x_3^2) \\ &= C_0 + x_3 C_1 + \frac{x_3^2}{2} C_2 + o(x_3^2). \end{aligned} \tag{11}$$

We note that since $y(x_1, x_2)$, $b(x_1, x_2)$, $c(x_1, x_2)$ and $d(x_1, x_2)$ do not depend on x_3, the same is true about F_i and C_i for $i = 0, 1, 2$. We also remark that depending on the smoothness of u, one can consider more terms in the expansion (6), and thus get higher-order expansions for F and C.

Combining now (2)–(4) and (11), and utilizing the symmetry of $\mathbb{C}$, we get

$$\begin{aligned} W(C, \theta) &= \frac{1}{8} (C - I(\theta)) \cdot \mathbb{C} (C - I(\theta)) \\ &= \frac{1}{8} \Big[(C_0 - I(\theta)) \cdot \mathbb{C} (C_0 - I(\theta)) + x_3 2\, (C_0 - I(\theta)) \cdot \mathbb{C} C_1 \\ &\qquad + x_3^2 \big[C_1 \cdot \mathbb{C} C_1 + (C_0 - I(\theta)) \cdot \mathbb{C} C_2 \big] \Big] + o(x_3^2) \quad \text{as } x_3 \to 0. \end{aligned}$$

Inserting the above expression into (5) and integrating out x_3 gives

$$\begin{aligned} \mathcal{E}_h(u, \theta) = \frac{h}{8} \int_\Omega \Big[&[C_0(x) - I(\theta(x))] \cdot \mathbb{C} [C_0(x) - I(\theta(x))] \\ &+ \frac{h^2}{12} \left[C_1(x) \cdot \mathbb{C} C_1(x) + [C_0(x) - I(\theta(x))] \cdot \mathbb{C} C_2(x) \right] \Big] \, dx \\ &+ o(h^3) \quad \text{as } h \to 0. \end{aligned} \tag{12}$$

In the expression above, $x = (x_1, x_2)$ and the integral is taken over the two-dimensional domain Ω, and it was assumed that the temperature, $\theta(x)$, was constant in the x_3 direction, which is reasonable for thin films. Note that, as expected, the energy is of order h, corresponding to the volume of the film. The energy consists of two main parts. The first term is a "membrane" energy of order h, which captures how much the dominant term of the right Cauchy–Green strain, C_0, deviates from the zero-energy state. The second term is an energy of order h^3, which can be interpreted as a "bending" energy. We shall discuss this term further in Section 4. We also note that if one further expanded C in (11) and used a third-order term C_3, this term would not affect the bending energy. Similarly, using a third-order term F_3 in the expansion (8) has no impact on C_0, C_1, and C_2, so the bending energy is now fully described in terms of F_0, F_1, F_2 and C_0, C_1, C_2.

If $\tilde{W}(E)$ in (4) is not necessarily a quadratic function of E, but is sufficiently smooth, then we can use the expansion of $\tilde{W}(E)$ (and hence that of $W(C)$) to expand

the energy as follows (we suppress the dependence on x for clarity) and obtain as $h \to 0$ the generalization of (12)

$$\begin{aligned}\mathcal{E}_h(u,\theta) &= h\int_\Omega \Bigg[\tilde{W}\left(\tfrac{1}{2}(C_0 - I(\theta))\right) \\ &\quad + \frac{h^2}{24}\left(\frac{1}{4}\,C_1 \cdot \frac{\partial^2 \tilde{W}}{\partial E^2}\bigg|_{E=\frac{1}{2}(C_0-I(\theta))} C_1 + \frac{1}{2}\,\frac{\partial \tilde{W}}{\partial E}\bigg|_{E=\frac{1}{2}(C_0-I(\theta))} \cdot C_2\right)\Bigg]\,dx \\ &\quad + o(h^3) \\ &= h\int_\Omega \left[W(C_0) + \frac{h^2}{24}\left(C_1 \cdot \frac{\partial^2 W}{\partial C^2}\bigg|_{C=C_0} C_1 + \frac{\partial W}{\partial C}\bigg|_{C=C_0} \cdot C_2\right)\right] dx \\ &\quad + o(h^3).\end{aligned} \tag{13}$$

Finally, as a special case, let us consider $C = C_0 + x_3 C_1 + \dfrac{x_3^2}{2} C_2$ in (11). The exact expression for the energy (12) is then

$$\begin{aligned}\mathcal{E}_h(u,\theta) &= \frac{h}{8}\int_\Omega \Big[[C_0(x) - I(\theta(x))] \cdot \mathbb{C}[C_0(x) - I(\theta(x))] \\ &\quad + \frac{h^2}{12}\left[C_1(x)\cdot\mathbb{C}C_1(x) + [C_0(x) - I(\theta(x))]\cdot\mathbb{C}C_2(x)\right] + \frac{h^4}{340}\,C_2(x)\cdot\mathbb{C}C_2(x)\Big]\,dx \\ &= \frac{h}{8}\int_\Omega \Big[[C_0(x) - I(\theta(x)) + \frac{h^2}{24}\,C_2(x)] \cdot \mathbb{C}[C_0(x) - I(\theta(x)) + \frac{h^2}{24}\,C_2(x)] \\ &\qquad + \frac{h^2}{12}\,C_1(x)\cdot\mathbb{C}C_1(x) + \frac{h^4}{720}\,C_2(x)\cdot\mathbb{C}C_2(x)\Big]\,dx.\end{aligned}$$

Since this last expression is written as a sum of three squares, it follows that zero-energy minimizers in this case would have to satisfy $C_1(x) = C_2(x) = 0$ and $C_0(x) = I(\theta(x))$ in Ω, giving rise to relevant compatibility conditions. If one considers the functions y, b, c, etc. as decoupled from each other, then these compatibility conditions can be interpreted in terms of the fundamental forms of the surface $y(x_1, x_2)$ [16]. For example, the first 2×2 block of C_0 is $(\nabla y)^T(\nabla y)$, and $C_0 = I(\theta)$ now gives a restriction on the first fundamental form. See the second half of Section 4 for a brief discussion regarding the second fundamental form. Clearly, these compatibility conditions are less restrictive than in the full 3D case, but we have not explored this issue (and the relevant Gauss–Codazzi–Mainardi equations) in greater depth.

4 Relationship to Γ-limit models

We next briefly discuss the relationship of the model from the previous section to those derived using Γ-convergence techniques. Such techniques give a rigorous meaning to the convergence of functionals (for general theory, see, e.g., [6,35]), and they have been useful in the asymptotic analyses of functionals that model the rescaled elastic energy of films as the thickness converges to zero [1, 3, 4, 14, 19, 22, 23, 34, 36, 44]. The limiting energies are two-dimensional and they can provide more tractable and efficiently computed models. In what follows, we shall only give a general discussion of the relationship between our model and those rigorously derived using Γ-convergence, and we refer the reader to the references above for further details.

First, notice that the expansion (8) has the leading term $F_0 = (\nabla y|b) = (y_{,1}|y_{,2}|b)$ by construction, and the "membrane" parts of the energies in (12) and (13) are functions of C_0, and hence F_0, only. In (8) both y and b are related to the original three-dimensional deformation u via (7), but in order to minimize these two-dimensional energies, these terms should be decoupled (as well as c and d). This correlates with the results obtained by applying Γ-convergence techniques.

In general, since the membrane energy of a film is proportional to the volume of the film, one usually linearly rescales the film to have thickness 1 and studies the Γ-limit as $h \to 0$ of the rescaled three-dimensional energy $\frac{1}{h}\mathcal{E}_h$ on the rescaled domain.

If the energy functional is defined as an integral of only an elastic energy density, W, which is viewed as a function of the deformation gradient, ∇u, then, under suitable assumptions on the energy density and the underlying space of admissible deformations u and its topology, it is possible to show that the Γ-limiting functional is two-dimensional (i.e., independent of the out-of-plane coordinate), and reduces to an integral of the quasiconvexification of an energy density $W_{3\times 2}$ defined on $\mathbb{R}^{3\times 2}$ via

$$W_{3\times 2}(A) = \min\{W(A|b) : \ b \in \mathbb{R}^3\}.$$

The two-dimensional energy is then given by $\mathcal{E}(y) = \int_\Omega QW_{3\times 2}(\nabla y)\,dx$, where the quasiconvexification of $W_{3\times 2}$ is defined as

$$QW_{3\times 2}(F) = \inf\left\{\frac{1}{|\Omega|}\int_\Omega W_{3\times 2}(F+\nabla\varphi)\,dx : \ \varphi \in C_0^1(\Omega;\mathbb{R}^3)\right\}.$$

This energy is then to be minimized with respect to y (see, e.g., [34]).

Sometimes a regularizing higher-gradient term is added to the three-dimensional energy functional to model, for instance, energy of interfaces between different phases of the material [4, 14, 44]. In those cases, passing the rescaled three-dimensional energy to the Γ-limit as $h \to 0$ yields a limiting two-dimensional energy that contains $\int_\Omega W(\nabla y|b)\,dx$ (plus a higher-gradient term or other terms). Notice that in both of the cases above a two-stage minimization is involved: minimizing with respect to b (which plays a role of the out-of-plane gradient), and minimizing with respect to y (which describes the deformation of the two-dimensional film). The minimizers y and b of the two-dimensional energy can in many cases be obtained as weak limits of $\{u_h\}$ and $\{u_{h,3}\}$, respectively, where $\{u_h\}$ is a subsequence of minimizers of the rescaled three-dimensional energy.

Work has been done recently to rigorously derive two-dimensional nonlinear theories for plates and shells [20–23, 41, 42]. In order to derive the Γ-limit of the bending energy, which scales like h^3, the behavior of the rescaled energy $\frac{1}{h^3}\int_{\Omega_h} W(\nabla u)\,dx$ is studied, where W is frame-indifferent, sufficiently smooth, nonnegative, and vanishing exactly on SO(3). If, in addition, one assumes a suitable simple growth condition from below, it can then be shown (see, e.g., [22]) that the Γ-limiting functional has the form proposed by G. Kirchhoff in 1850 [32]

$$\mathcal{E}(y) = \begin{cases} \frac{1}{24}\int_\Omega Q_2(\mathrm{II})\,dx & \text{if } y \in W^{2,2}(\Omega;\mathbb{R}^3) \text{ is an isometry} \\ & \text{(i.e., } |y_{,1}| = |y_{,2}| = 1,\ y_{,1}\cdot y_{,2} = 0), \\ +\infty & \text{otherwise.} \end{cases} \tag{14}$$

In the above, II is the second fundamental form of the surface given by

$$\mathrm{II}_{ij} = y_{,i}\cdot(y_{,1}\times y_{,2})_{,j}.$$

Q_2 is defined for $G \in \mathbb{R}^{2\times 2}$ via

$$Q_2(G) = \min\left\{Q_3(\hat{G}|v) :\ v \in \mathbb{R}^3\right\}, \quad \text{where } \hat{G} = \begin{bmatrix} G_{11} & G_{12} \\ G_{21} & G_{22} \\ 0 & 0 \end{bmatrix} \tag{15}$$

and

$$Q_3(H) = H \cdot \frac{\partial^2 W}{\partial F^2}\bigg|_{F=I} H \quad \text{for } H \in \mathbb{R}^{3\times 3}.$$

In order to relate the above result to our model, we should assume that the temperature of the film is constant and low enough so that $f(\theta) = 0$ in (1) and $I(\theta) = I$, and that the membrane part of the energy is zero. The membrane energy is zero if and only if $C_0 = I(\theta)$. Since $C_0 = F_0^T F_0$ and $F_0 = (\nabla y|b)$, the membrane energy being zero translates to the conditions

$$\begin{aligned} |y_{,1}| = |y_{,2}| = |b| = 1, \\ y_{,1} \cdot y_{,2} = y_{,1} \cdot b = y_{,2} \cdot b = 0. \end{aligned}$$

In particular, y is an isometry and b is the unit normal to the surface. In addition, $b = y_{,1} \times y_{,2}$ by virtue of $\det C_0 = 1$. The bending energy in (13) now reduces to

$$\mathcal{E}_{\text{bending}} = \frac{h^3}{24} \int_\Omega C_1 \cdot \frac{\partial^2 W}{\partial C^2}\bigg|_{C=I} C_1, \tag{16}$$

where we recall from (9) and (10) that

$$\begin{aligned} C_1 &= F_0^T F_1 + F_1^T F_0 \\ &= (y_{,1}|y_{,2}|b)^T (b_{,1}|b_{,2}|c) + (b_{,1}|b_{,2}|c)^T (y_{,1}|y_{,2}|b) \\ &= \begin{bmatrix} \mathrm{II}_{11} & \mathrm{II}_{12} & y_{,1}\cdot c \\ \mathrm{II}_{21} & \mathrm{II}_{22} & y_{,2}\cdot c \\ 0 & 0 & b\cdot c \end{bmatrix} + \begin{bmatrix} \mathrm{II}_{11} & \mathrm{II}_{12} & y_{,1}\cdot c \\ \mathrm{II}_{21} & \mathrm{II}_{22} & y_{,2}\cdot c \\ 0 & 0 & b\cdot c \end{bmatrix}^T. \end{aligned}$$

In the above, we used the fact that since $|b| = 1$, we also have $b \cdot b_{,i} = 0$ for $i = 1, 2$. Note that

$$\begin{aligned} Q_3(H) &= H \cdot \frac{\partial^2 W(F^T F)}{\partial F^2}\bigg|_{F=I} H \\ &= (H + H^T) \cdot \frac{\partial^2 W}{\partial C^2}\bigg|_{C=I} (H + H^T), \end{aligned}$$

and hence

$$C_1 \cdot \frac{\partial^2 W}{\partial C^2}\bigg|_{C=I} C_1 = Q_3\left(\begin{bmatrix} \mathrm{II}_{11} & \mathrm{II}_{12} & y_{,1}\cdot c \\ \mathrm{II}_{21} & \mathrm{II}_{22} & y_{,2}\cdot c \\ 0 & 0 & b\cdot c \end{bmatrix}\right).$$

Since $\{y_{,1}, y_{,2}, b\}$ form an orthonormal system in $\mathbb{R}^3$, we can view $y_{,1} \cdot c$, $y_{,2} \cdot c$, and $b \cdot c$ as independent variables and minimize them out as in the definition of Q_2 in (15). Thus, the asymptotically derived bending energy (16) agrees formally with the bending energy (14) obtained by using Γ-convergence techniques.

It is noted in [22] that for the special case of an isotropic material, minimizing out v in (15) yields the Γ-limiting functional of the form

$$\mathcal{E}(y) = \begin{cases} \dfrac{1}{24}\displaystyle\int_\Omega \left(\frac{2\lambda\mu}{\lambda+2\mu}(\operatorname{tr} \mathrm{II})^2 + 2\mu|\mathrm{II}|^2 \right) dx & \text{if } y \in W^{2,2}(\Omega;\mathbb{R}^3) \text{ is an isometry,} \\ +\infty & \text{otherwise,} \end{cases}$$

which turns out to be the same as the bending energy in Koiter's shell model in the next section.

5 Comparison to Koiter's shell model

We now briefly discuss the similarities and differences between our model and Koiter's shell model [16,33], which has become a computationally popular model for shells and plates as it combines both a membrane and a bending energy. Since our reference configuration is flat, we shall only compare our model to the corresponding plate case of Koiter's model with a flat reference configuration. Unlike our model, Koiter's model only deals with a deformation of the middle surface of the shell/plate, so the reference configuration is the two-dimensional domain $\Omega \subset \mathbb{R}^2$. The first fundamental form (the 2×2 equivalent of the right Cauchy–Green strain) of the reference configuration is the identity matrix $I_2 \in \mathbb{R}^{2\times 2}$, and the second fundamental form is identically zero. For the deformed configuration, $y(\Omega)$, the components of the first and second fundamental forms are given by $(\alpha, \beta = 1, 2)$

$$\mathrm{I}_{\alpha\beta} = C_{\alpha\beta} = y_{,\alpha} \cdot y_{,\beta}\,, \qquad \text{and} \qquad \mathrm{II}_{\alpha\beta} = y_{,\alpha} \cdot n_\beta \quad \text{with } n = \frac{y_{,1} \times y_{,2}}{|y_{,1} \times y_{,2}|}.$$

If one now defines the "change of metric tensor", G, to be one half of the difference between the first fundamental forms, $G = \frac{1}{2}(\mathrm{I} - I_2)$, and a "change of curvature tensor", R, to be the difference between the second fundamental forms, $R = \mathrm{II}$, then, for a film of thickness 2ε, the energy functional proposed by Koiter takes the form (see [16])

$$\mathcal{E}_K(y) = \frac{1}{2}\int_\Omega \left[\varepsilon a^{\alpha\beta\sigma\tau} G_{\alpha\beta}(y) G_{\sigma\tau}(y) + \frac{\varepsilon^3}{3} a^{\alpha\beta\sigma\tau} R_{\alpha\beta}(y) R_{\sigma\tau}(y) \right] dx,$$

where (with δ_{ij} being the Kronecker delta)

$$a^{\alpha\beta\sigma\tau} = \frac{4\lambda\mu}{\lambda+2\mu}\delta_{\alpha\beta}\delta_{\sigma\tau} + 2\mu(\delta_{\alpha\sigma}\delta_{\beta\tau} + \delta_{\alpha\tau}\delta_{\beta\sigma}).$$

For $h = \varepsilon/2$ and after some simplifications, this energy functional becomes

$$\mathcal{E}_K(y) = \int_\Omega \left[\frac{h}{2}\left(\frac{2\lambda\mu}{\lambda+2\mu}(\operatorname{tr} G)^2 + 2\mu|G|^2 \right) + \frac{h^3}{24}\left(\frac{2\lambda\mu}{\lambda+2\mu}(\operatorname{tr} \mathrm{II})^2 + 2\mu|\mathrm{II}|^2 \right) \right] dx.$$

Note that the h^3-part of the energy agrees with the bending energy derived by Γ-convergence methods and given at the end of Section 4, so under the same assumptions as in Section 4, the bending energy in Koiter's model agrees with the bending energy in our model.

On the other hand, the membrane energy part of $\mathcal{E}_K$ does not agree with that in our model, even if one uses as a starting point the quadratic isotropic energy density

$\frac{1}{2}E\cdot\mathbb{C}E=\frac{1}{2}\left[\lambda(\operatorname{tr}E)^2+2\mu|E|^2\right]$. The membrane energy density in our 3D model just before integrating out x_3 is a function of the strain E of the form

$$E=\frac{1}{2}(C_0-I_3)=\frac{1}{2}\left(\begin{bmatrix}|y_{,1}|^2 & y_{,1}\cdot y_{,2} & y_{,1}\cdot b\\ y_{,1}\cdot y_{,2} & |y_{,2}|^2 & y_{,2}\cdot b\\ y_{,1}\cdot b & y_{,2}\cdot b & |b|^2\end{bmatrix}-I_3\right),$$

and therefore, if b is assumed to be the unit normal vector to the deformed configuration $y(\Omega)$, then $\operatorname{tr}E=\operatorname{tr}G$ and $|E|=|G|$ with G as above, so that the membrane energy density in our model (after integrating out x_3) becomes

$$\frac{h}{2}\left(\lambda\left(\operatorname{tr}G\right)^2+2\mu|G|^2\right),$$

which is different from the membrane energy of $\mathcal{E}_K$. However, if one was allowed to minimize out the vector b (which, of course, would then affect the bending energy part!), then one obtains, similarly as discussed at the end of Section 4, that the energy density is

$$\frac{h}{2}\left(\frac{2\lambda\mu}{\lambda+2\mu}\left(\operatorname{tr}G\right)^2+2\mu|G|^2\right),$$

agreeing with Koiter's model.

A few additional differences are worth pointing out. First, the derivation of Koiter's model starts out assuming that stresses away from the middle surface are planar and parallel to the middle surface. In our model, no *a priori* assumptions are placed on the vectors y, b, etc. in the expansion $u(x_1,x_2,x_3)=y(x_1,x_2)+x_3b(x_1,x_2)+\dots$ as defined in Section 3 (for example, b does not necessarily remain normal to the deformed surface, nor does it have to remain unit). From a computational point of view, both the membrane energy and the bending energy are easier to evaluate with a vector $b(x_1,x_2)$ independent of $y(x_1,x_2)$, than if it were the vector $b(x_1,x_2)=\dfrac{y_{,1}\times y_{,2}}{|y_{,1}\times y_{,2}|}$, so we feel that our model allows for more flexibility than Koiter's model. In addition, in our model higher-order terms in powers of h can be retained in the energy for additional corrections when the thickness h of the film becomes more significant. Finally, it is straightforward to extend our model to non-isotropic materials by modifying the energy density in (13).

6 Numerical results

In this section, we present numerical results for a variety of static heating programs applied to square free-standing films. After rescaling the dimensions of the film, we may assume that $\Omega=(0,1)\times(0,1)$ with the thickness of the film, h, rescaled appropriately. The energy to be minimized is given by the first two terms of (12),

$$\begin{aligned}\mathcal{E}_h(u,\theta)=\frac{h}{8}\int_\Omega\Big[&[C_0(x)-I(\theta(x))]\cdot\mathbb{C}[C_0(x)-I(\theta(x))]\\&+\frac{h^2}{12}\left[C_1(x)\cdot\mathbb{C}C_1(x)+[C_0(x)-I(\theta(x))]\cdot\mathbb{C}C_2(x)\right]\Big]\,dx.\end{aligned}\tag{17}$$

For simplicity, the sought deformation, $u(x_1,x_2,x_3)$, shall be approximated by the first two terms, $y(x_1,x_2)$ and $b(x_1,x_2)$, in (7), i.e., we shall assume that $u(x_1,x_2,x_3)=$

$y(x_1, x_2) + x_3 b(x_1, x_2)$ and minimize the energy (17) with respect to y and b, viewed as two independent functions related only via the energy (17). The function y describes the deformation of the middle section of the film (where $x_3 = 0$); the function b is sometimes referred to as a Cosserat vector describing the deformation of the cross-sections of the film. We shall use triangular finite element methods to minimize the energy; in the computational results described below, the domain Ω was divided into 128×128 squares and each square then subdivided into 2 triangles. On these meshes, the function y shall be approximated by the quadratic Morley finite element and the function b by a continuous piecewise linear element [7, 15]. With this choice of finite elements, the energy (17) becomes an integral of piecewise quartic polynomials. To perform the quadrature exactly, we shall use the 7-point Gaussian quadrature rule described in [17] and exact for polynomials of degree 5. Finally, the energy shall be minimized by a variant of the Fletcher–Reeves conjugate gradient algorithm [24,43] that has been used successfully by one of the authors to minimize similar energy functionals in [8–13].

From the discussion in Section 2 it follows that we can assume that our Melinex® material is isotropic and hence its elastic properties are fully described by its Young's modulus and its Poisson's ratio. We shall make the simplifying assumption that these material constants do not change with temperature. Representative values of Young's modulus and Poisson's ratio are 3 GPa and 0.35, respectively, and these values shall be used in all subsequent numerical results.[3]

The function $f(\theta)$ introduced in (1) via the identity $I(\theta) = (1 - f(\theta))I$ for the energy-minimizing Cauchy–Green strain can be obtained as follows. The discussion in Section 2 suggests that a uniformly heated material shrinks uniformly in all directions. For such deformations, the deformation gradient is constant, and, by the polar decomposition theorem, we have $F = RU$ with $R \in \mathrm{SO}(3)$ and $U = (1 - s(\theta))I$ being a diagonal matrix with diagonal entries of the form $1 - s(\theta)$, where $s(\theta)$ is the amount of shrinkage at the temperature θ. Referring to Figures 1 and 2, it is reasonable to assume that $s(\theta)$ can be approximated by a piecewise linear function of the form

$$s(\theta) = \begin{cases} 0 & \text{for } \theta \le 80, \\ \dfrac{\theta - 80}{700} & \text{for } 80 < \theta \le 150, \end{cases}$$

so that there is no shrinkage at 80°C, 10% shrinkage at 150°C, and the shrinkage is linear between 80°C and 150°C. Hence, at the temperature θ, the energetically preferred Cauchy–Green strain is

$$I(\theta) = F^T F = (1 - s(\theta))^2 I = (1 - f(\theta))I,$$

where $f(\theta) = 2s(\theta) - s^2(\theta)$.

We shall now describe several of the computational results. Since any nonconstant distribution of temperature cannot be handled by standard methods of thermodynamics, one might expect a certain prevalent mechanism of heat transfer for our system.

[3] The values of Young's modulus and Poisson's ratio have been measured by 3M. The modulus was obtained from tensile tests performed on the film at ambient conditions and at a strain rate of 10%/min. The Poisson's ratio was obtained from measurements performed on a different but similar PET material. That measurement itself was also a tensile test but the specimen was patterned and the Poisson's ratio determined using digital image correlation to measure both the longitudinal and transverse strains during the test. The Poisson's ratio was then determined from the negative slope of a plot of the transverse versus longitudinal strain.

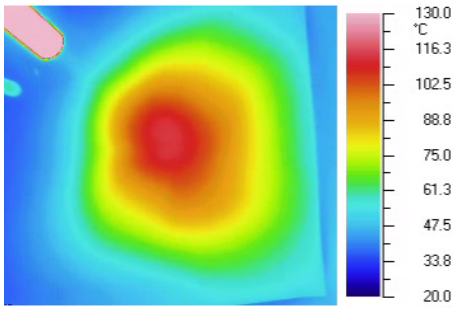

Fig. 3 An experimentally obtained temperature distribution obtained by aiming a heat gun at the center of a square film. Notice the heat gun in the upper left corner.

Some of our simulations correspond to aiming a hot-air gun, or a heat gun, at particular points on the surface of the film. With a heat gun, the primary mechanism of delivering heat to the film is by radiation, and the heat is removed by conduction, which is a much slower process than radiation [48]. For this reason, we shall assume that we can temporarily "freeze" the temperature distribution in the film and that it corresponds to a reasonable heat distribution generated by a heat gun. An example of a temperature distribution within the film resulting from using a heat gun is shown in Figure 3.

The first three sets of results (Figures 4, 5, and 6) correspond to aiming a heat gun at a particular point on the surface of the film. The results in Figure 4 can be thought of as corresponding to the heat gun being aimed at the center of the film and being "far" from the surface of the film, so that the heat/temperature profile is more diffused and the temperature at the center of the film is lower compared to the results in Figure 5, which can be thought of as having a more focused heat gun closer to the film (still pointing at the center) so that the temperature is higher at the center of the film. The results in Figure 6 correspond to the same, focused beam of heat as in Figure 5, but this time aimed at the center of the upper left quarter of the film. The temperature distributions are assumed to be Gaussian with the maximum temperatures being 100°C for the results in Figure 4 and 120°C for the results in Figures 5 and 6. For the more diffused distribution in Figure 4, the temperature is 80°C for points along the circle of radius 0.5 away from the center of the film, and for Figures 5 and 6 it is 80°C for points along the circle of radius 0.15 away from the point experiencing the highest temperature. All three temperature distributions are offset by 20°C (assumed to be the room temperature). Mathematically, the results in Figure 4 correspond to the temperature function

$$\theta(x_1, x_2) = 20 + 80 \exp\left(-\frac{(x_1 - 0.5)^2 + (x_2 - 0.5)^2}{0.15^2} \log\frac{80}{60}\right), \tag{18}$$

the results in Figure 5 to

$$\theta(x_1, x_2) = 20 + 100 \exp\left(-\frac{(x_1 - 0.5)^2 + (x_2 - 0.5)^2}{0.15^2} \log\frac{100}{60}\right), \tag{19}$$

and the results in Figure 6 to

$$\theta(x_1, x_2) = 20 + 100 \exp\left(-\frac{(x_1 - 0.25)^2 + (x_2 - 0.75)^2}{0.15^2} \log\frac{100}{60}\right). \tag{20}$$

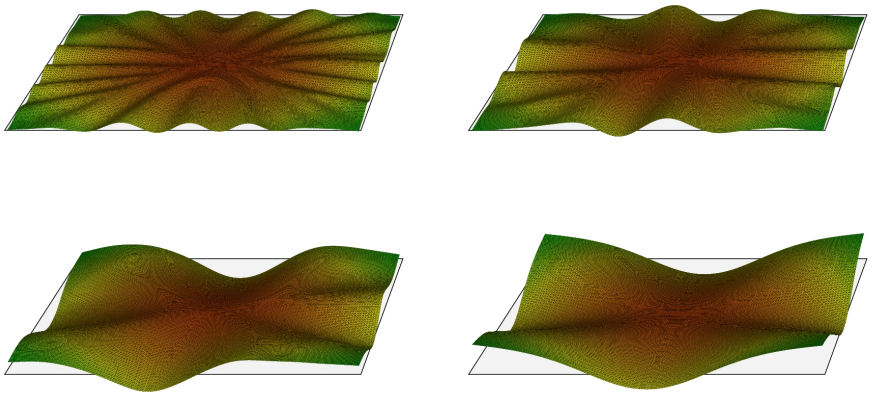

Fig. 4 Computed deformations for the temperature distribution (18) and thicknesses of 12.5 μm, 50 μm, 100 μm, and 500 μm for a square film of size 20 cm by 20 cm.

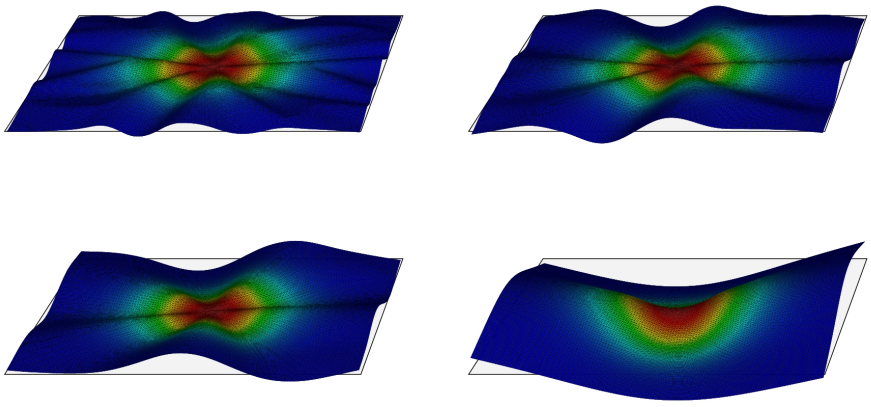

Fig. 5 Computed deformations for the temperature distribution (19) and thicknesses of 12.5 μm, 50 μm, 100 μm, and 500 μm for a square film of size 20 cm by 20 cm.

In all of the Figures 4–8, the yellow color corresponds to 80°C, the lowest temperature above which shrinkage should occur. Each figure displays four computational results, corresponding, in physical units, to square films with the square base of size 20 cm by 20 cm, and with four different thicknesses: 12.5 μm and 50 μm in the upper row, and 100 μm and 500 μm in the lower row. We note that the results corresponding to Figures 4–6 are conceptually very similar. Shrinkage should occur inside a circle, and the amount of shrinkage decreases as the distance from the center of the circle increases. Hence, there is a competition between the circular region, where, from the energetical

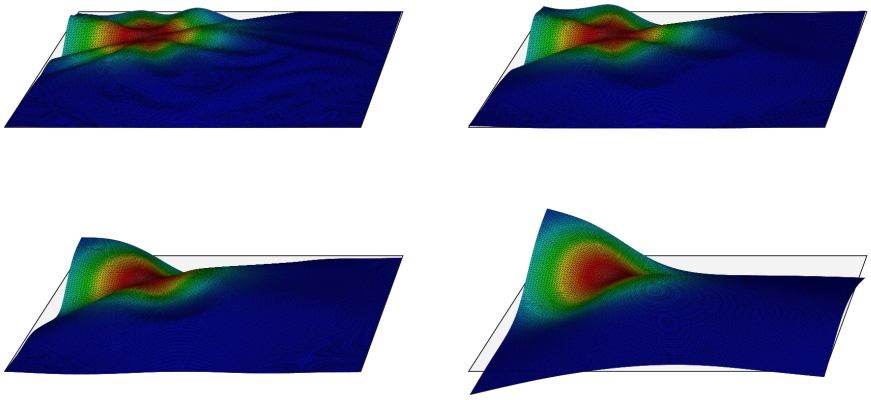

Fig. 6 Computed deformations for the temperature distribution (20) and thicknesses of 12.5 μm, 50 μm, 100 μm, and 500 μm for a square film of size 20 cm by 20 cm.

point of view, shrinkage is preferred, and the surrounding region that prefers to stay in the unshrunk form.

The results in Figure 7 correspond to heating two opposite edges of the film so that the film prefers to shrink inside of two narrow strips along the two edges while trying to stay in the unshrunk form in the wide center strip. The temperature profile is constructed as a combination of two Gaussians

$$\theta(x_1, x_2) = 20 + 80\left[\exp\left(-\frac{x_2^2}{0.25^2}\,\log\frac{160}{60}\right) + \exp\left(-\frac{(1-x_2)^2}{0.25^2}\,\log\frac{160}{60}\right)\right]. \quad (21)$$

The temperature along the edges $x_2 = 0$ and $x_2 = 1$ is $\approx 100^\circ$C, along the center line $x_2 = 0.5$ it is $\approx 23^\circ$C, and it is $\approx 80^\circ$C along the lines $x_2 = 0.135$ and $x_2 = 0.865$. As expected, for small thicknesses there is a significant number of pleats extending from the edges experiencing the high temperatures into the low-temperature region. As the thickness of the film increases, the bending energy increases for a particular deformation, so, as a result, the number of pleats in the deformed configuration decreases. We observe that for the film of thickness 500 μm there are no visible pleats and the film has deformed into a shape that appears to have positive Gaussian curvature everywhere. We note that when this resulting deformation was used as an initial guess for the deformations corresponding to smaller thicknesses, the resulting energy-minimizing deformations looked very similar, suggesting that one should be able to bend (without much or any stretching) the deformed films corresponding to smaller thicknesses to the shape corresponding to the thicker one.

Finally, let us discuss the results in Figure 8. In this case, the center line $x_2 = 0.5$ is heated to $\approx 130^\circ$C, while the edges $x_2 = 0$ and $x_2 = 1$ experience the lowest temperature of $\approx 80^\circ$C. More precisely, the temperature distribution is given by

$$\theta(x_1, x_2) = 80 + 700\,(1.0 - a\cosh(b\,(x_2 - 0.5)))\,, \quad (22)$$

where $a \approx 0.92857$ and $b \approx 0.77952$. In this case, since the temperature is greater than or equal to 80°C everywhere, the whole surface will experience shrinkage. The

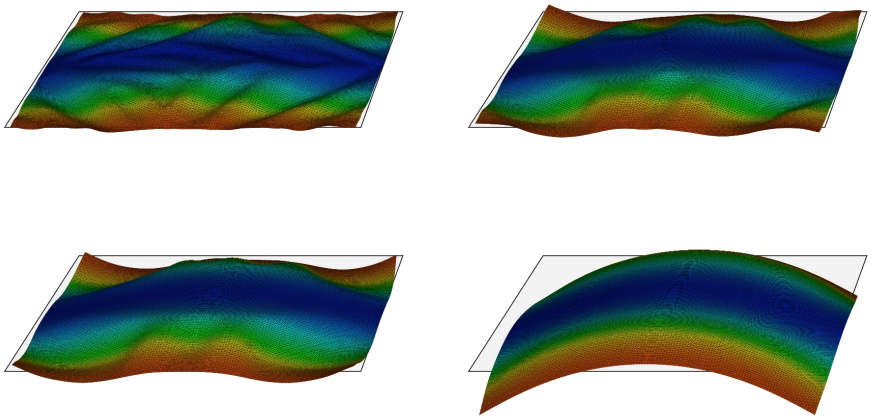

Fig. 7 Computed deformations for the temperature distribution (21) and thicknesses of 12.5 μm, 50 μm, 100 μm, and 500 μm for a square film of size 20 cm by 20 cm.

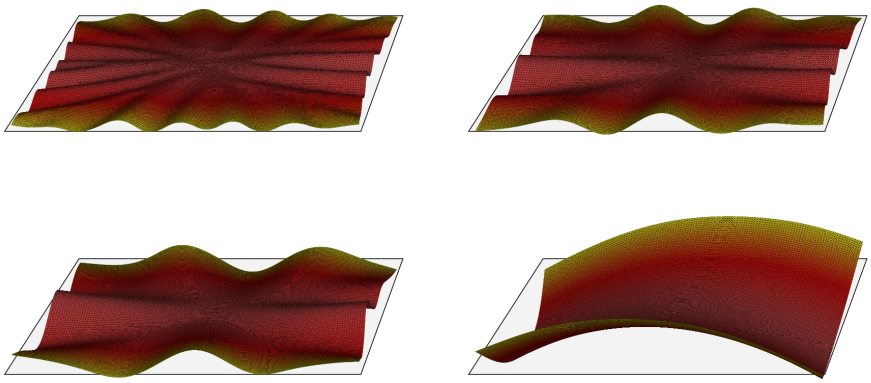

Fig. 8 Computed deformations for the temperature distribution (22) and thicknesses of 12.5 μm, 50 μm, 100 μm, and 500 μm for a square film of size 20 cm by 20 cm.

center strip near the line $x_2 = 0.5$ is being shrunk the most, with shrinkage of about 7%, while the edges $x_2 = 0$ and $x_2 = 1$ should undergo zero shrinkage barring any elastic competition effects. We see in Figure 8 that the film again exhibits the most wrinkling for smaller thicknesses and, as expected, the wrinkles start to disappear as the thickness of the film increases. For the 500 μm film, there is no apparent wrinkling and all of the curvature is distributed quite evenly over the whole surface. In this case, the surface appears to have negative Gaussian curvature everywhere and a shape of a catenoid. Again, when this resulting deformation was used as an initial guess for the deformations corresponding to smaller thicknesses, the resulting energy-minimizing

deformations again looked very similar, suggesting that one should be able to bend the deformed films corresponding to smaller thicknesses to the catenoidal shape.

7 Conclusions

In this paper, we have proposed a simple mathematical model for the behavior of a class of heat-shrinkable polymer-based thin films represented by a DuPont's Melinex® polyester film. Based on experiments, it has been determined that these materials behave more-or-less isotropically and exhibit shrinkage that depends on the highest temperature the film has been exposed to. Using the concept of a "preferred" Cauchy–Green strain for a given high temperature in the material's history, we defined a three-dimensional energy for the material that depends on the amount of additional strain. Using asymptotic expansions for the deformation, its gradient, its right Cauchy–Green strain, and the energy functional, we were able to obtain a two-dimensional energy, whose lowest-order terms can be interpreted as a membrane energy and a bending energy, respectively. This energy was then compared to those obtained by using Γ-convergence techniques and that in Koiter's shell model, and agreement was found in the bending energies under some *a priori* unifying assumptions, while a slight disagreement was found between all of the membrane energies. Finally, using the developed model, numerical results have been presented for various temperature distributions applied to free-standing films, and a qualitative agreement was found with experimental results. In addition, it was demonstrated that various possible deformations are possible that include those with everywhere positive or everywhere negative Gaussian curvature.

Acknowledgements This work was supported in part by a University of St. Thomas Research Assistance Grant. We are also greatly indebted to Roger Fosdick for many fruitful discussions and numerous suggestions on how to make this work better, and to David Steigmann, who has provided several valuable suggestions and directed us to work we were not aware of.

References

1. E. Acerbi, G. Buttazzo, and D. Percivale. A variational definition for the strain energy of an elastic string. *J. Elasticity*, 25:137–148, 1991.
2. S. S. Antman. *Nonlinear Problems of Elasticity*. Springer-Verlag, New York, 1995.
3. G. Anzellotti, S. Baldo, and D. Percivale. Dimension reduction in variation problems, asymptotic development in Γ-convergence and thin structures in elasticity. *Asympt. Anal.*, 9:61–100, 1994.
4. K. Bhattacharya and R. D. James. A theory of thin films of martensitic materials with applications to microactuators. *J. Mech. Phys. Solids*, 47(3):531–576, 1999.
5. G. Bouchitté, I. Fonseca, and M. L. Mascarenhas. Bending moment in membrane theory. *J. Elasticity*, 73:75–99, 2003.
6. A. Braides. *Γ-convergence for Beginners*. Oxford University Press, Oxford, 2002.
7. S. C. Brenner and L. R. Scott. *The Mathematical Theory of Finite Element Methods*. Springer-Verlag, New York, 1994.
8. P. Bělík, T. Brule, and M. Luskin. On the numerical modeling of deformations of pressurized martensitic thin films. *M2AN Math. Model. Numer. Anal.*, 35(3):525–548, 2001.
9. P. Bělík and M. Luskin. A computational model for the indentation and phase transformation of a martensitic thin film. *J. Mech. Phys. Solids*, 50(9):179–1815, 2002.
10. P. Bělík and M. Luskin. A total-variation surface energy model for thin films of martensitic crystals. *Interfaces Free Bound.*, 4:71–88, 2002.

11. P. Bělík and M. Luskin. A computational model for martensitic thin films with compositional fluctuation. *Math. Models Methods Appl. Sci.*, 14(11):1585–1598, 2004.
12. P. Bělík and M. Luskin. Computational modeling of softening in a structural phase transformation. *Multiscale Model. Simul.*, 3:764–781, 2005.
13. P. Bělík and M. Luskin. Computation of the training of a martensitic thin film. *Calcolo*, 43:197–215, 2006.
14. P. Bělík and M. Luskin. The Γ-convergence of a sharp interface thin film model with non-convex elastic energy. *SIAM J. Math. Anal.*, 38:414–433, 2006.
15. P. Ciarlet. *The Finite Element Method for Elliptic Problems*. North-Holland, Amsterdam, 1978.
16. P. G. Ciarlet. An introduction to differential geometry with applications to elasticity. *J. Elasticity*, 78–79(1):3–201, 2005.
17. D. A. Dunavant. High degree efficient symmetrical Gaussian quadrature rules for the triangle. *Internat. J. Numer. Methods Engrg.*, 21:1129–1148, 1985.
18. W. N. Findley, J. S. Lai, and K. Onaran. *Creep and Relaxation of Nonlinear Viscoelastic Materials*. North Holland, Amsterdam, 1976.
19. I. Fonseca and G. Francfort. 3D-2D asymptotic analysis of an optimal design problem for thin films. *J. Reine Angew. Math*, 505:173–202, 1998.
20. G. Friesecke, R. D. James, M. G. Mora, and S. Müller. Derivation of nonlinear bending theory for shells from three-dimensional nonlinear elasticity by Gamma-convergence. *C. R. Acad. Sci. Paris, Sér. I*, 336:697–702, 2003.
21. G. Friesecke, R. D. James, and S. Müller. The Föppl–von Kármán plate theory as a low energy Γ-limit of nonlinear elasticity. *C. R. Acad. Sci. Paris, Sér. I*, 332:1–6, 2002.
22. G. Friesecke, R. D. James, and S. Müller. A theorem on geometric rigidity and the derivation of nonlinear plate theory from three dimensional elasticity. *Comm. Pure Appl. Math.*, 55:1461–1506, 2002.
23. G. Friesecke, R. D. James, and S. Müller. A hierarchy of plate models derived from nonlinear elasticity by Gamma-convergence. *Arch. Rational Mech. Anal.*, 180(2):183–236, 2006.
24. R. Glowinski. *Numerical Methods for Nonlinear Variational Problems*. Springer-Verlag, New York, 1984.
25. Y. Grabovsky and L. Truskinovsky. The flip side of buckling. *Contin. Mech. Thermodyn.*, 19(3–4):211–243, 2007.
26. P. Gudmundson. A unified treatment of strain gradient plasticity. *J. Mech. Phys. Solids*, 52:1379–1406, 2004.
27. M. E. Gurtin. *Topics in Finite Elasticity*. SIAM, Philadelphia, 1981.
28. M. E. Gurtin. A gradient theory of single-crystal viscoplasticity that accounts for geometrically necessary dislocations. *J. Mech. Phys. Solids*, 50:5–32, 2002.
29. M. G. Hilgers and A. C. Pipkin. Bending energy of highly elastic membranes. *Q. Appl. Math.*, 50(2):389–400, 1992.
30. M. G. Hilgers and A. C. Pipkin. Bending energy of highly elastic membranes ii. *Q. Appl. Math.*, 54(2):307–316, 1996.
31. P. Hornung. A Γ-convergence result for thin martensitic films in linearized elasticity. *SIAM J. Math. Anal.*, 40:186–214, 2008.
32. G. Kirchhoff. Über das Gleichgewicht und die Bewegung einer elastischen Scheibe. *J. Reine Angew. Math.*, 40:51–88, 1850.
33. W. T. Koiter. On the nonlinear theory of thin elastic shells. *Proc. Kon. Ned. Akad. Wetensch.*, B69:1–54, 1966.
34. H. Le Dret and A. Raoult. The nonlinear membrane model as variational limit of nonlinear three-dimensional elasticity. *J. Math. Pures Appl.*, 73:549–578, 1995.
35. G. D. Maso. *An Introduction to Γ-convergence*. Birkhäuser, 1993.
36. L. Modica and S. Mortola. Il limite nella Γ-convergenza di una famiglia di funzionali ellittici. *Boll. Un. Mat. Ital. A (5)*, 14(3):526–529, 1977.
37. P. Neff. Local existence and uniqueness for a geometrically exact membrane-plate with viscoelastic transverse shear resistance. *Math. Methods Appl. Sci*, 28(9):1031–1060, 2005.
38. L. Nicola, Y. Xiang, J. J. Vlassak, E. V. der Giessen, and A. Needleman. Plastic deformation of freestanding thin films: Experiments and modeling. *J. Mech. Phys. Solids*, 54:2089–2110, 2006.
39. K. Osaki. Constitutive equations and damping function for entangled polymers. *Korea–Australia Rheology Journal*, 11(4):287–291, 1999.

40. A. Oza, R. Vanderby, and R. S. Lakes. Interrelation of creep and relaxation for nonlinearly viscoelastic materials: application to ligament and metal. *Rheol. Acta*, 42:557–568, 2003.
41. O. Pantz. Une justification partielle du modèle de plaque en flexion par Γ-convergence. *C. R. Acad. Sci. Paris, Sér. I*, 332:587–592, 2001.
42. O. Pantz. On the justification of the nonlinear inextensional plate model. *Arch. Rational Mech. Anal.*, 167:179–209, 2003.
43. E. Polak. *Computational Methods in Optimization.* Academic Press, New York, 1971.
44. Y. C. Shu. Heterogeneous thin films of martensitic materials. *Arch. Rational Mech. Anal.*, 153:39–90, 2000.
45. J. Sorvari and M. Malinen. Determination of the relaxation modulus of a linearly viscoelastic material. *Mechanics of Time-Dependent Materials*, 10:125–133, 2006.
46. D. J. Steigmann. Asymptotic finite-strain thin-plate theory for elastic solids. *Comput. Math. Appl.*, 53:287–295, 2007.
47. D. J. Steigmann. Thin-plate theory for large elastic deformations. *Internat. J. Non-Linear Mech.*, 42:233–240, 2007.
48. G. S. Zhdanov. Experimental investigation of the temperature distribution in thin films heated by an electron beam. *J. Engrg. Phys. Thermophys.*, 21(6):1557–1561, 1971.